Tunable Diode Laser Absorption Spectroscopy and its Application in an Impulse Hypervelocity Facility

J. M. Meyers
AERONAUTICS AND AEROSPACE DEPARTMENT
VON KARMAN INSTITUTE FOR FLUID DYNAMICS

Tunable diode laser absorption spectroscopy (TDLAS) is a technique that has potential to acquire temperature, pressure and specie density along with velocity measurements in many gas-dynamic environments making it a valuable tool for flow diagnostics. The work contained in this report is aimed to give readers a base knowledge in the application of TDLAS. Methods in how to extract thermodynamic information (temperature, pressure, specie density), how to measure velocity (via Doppler shift) and how to improve signal quality for low-level absorption conditions will be addressed. An application of this technique focuses on the development of a sensor to monitor the low-temperature and low-pressure ($\sim$100K, $\sim$2torr) hyper-velocity ($\sim$1750m/s) free-stream flow of the Longshot free-piston impulse ($\sim$40msec) hypervelocity facility.

1 Introduction

1.1 Near-Infrared Absorption Spectroscopy

Spectroscopy is the study of how light and matter interact with one another. It is a broad and complex science. Even a very simple molecule can give a very complex spectrum. Fortunately, the entire spectra of a molecule need not be known to identify important thermodynamic characteristics. The near-infrared (NIR) is a key location for finding ro-vibrational transitions of many atmospheric and combustion species and thanks to the booming telecommunications industry, many types of laser sources have become quite affordable for NIR laser spectroscopy. A ro-vibrational transition is one in which a rotational transition occurs within a vibrational band. Position of these vibrational bands and the rotational line transitions are determined by the spacing of the energy levels which are dependent upon quantum selection rules. Figure 1 illustrations individual rotation transition spacings from a lower rotational state, J'' in a lower vibrational band , ν'', to a higer rotational state, J'', in a higher vibrational band, ν'. The widths and spectral and intensity of these spectral lines depend on many parameters including gas type, thermodynamic properties (temperature and pressure), population of states, pathlength, etc. An understanding of how these statistical and classical thermodynamic concepts relate is the keystone to spectroscopic techniques.

A simple direct absorption spectroscopy experiment is illustrates this concept in figure 2. In this figure, a light source at initial intensity, I_0, passes through an absorbing medium yield a transmitted intensity, I.
THe absorption can be calculated using equation 1 which represents the Beer-Lambert law that relates absorption, $\alpha(\nu) L$, with a reference intensity, I_0, and a transmitted intensity, I.

$$-\alpha(\nu) L = ln\left(\frac{I}{I_0}\right) \tag{1}$$

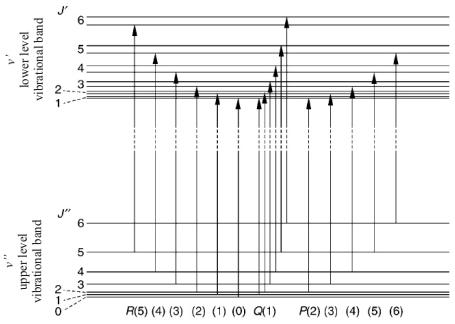

Figure 1: Illustration of ro-vinrational transition band make-up

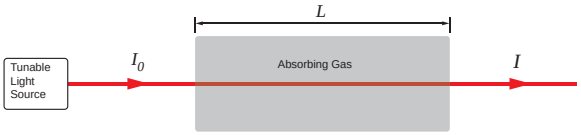

Figure 2: Simple absorption illustration

This simple relation can be seen in figure 3 where a simulated non-linear reference signal, I_0, and a transmitted intensity with four absorption features present, I, are used to acquire the direct absorption.

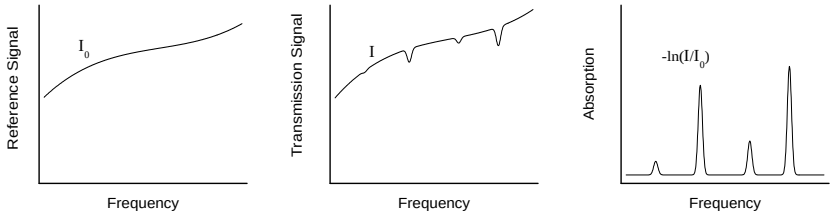

Figure 3: Simple absorption calculation

The absorption coefficient, $\alpha(\nu)$ for multiple gas species is defined as:

$$\alpha(\nu) = P \sum_{j=1}^{k} \left(X_j \sum_{i=1}^{N_j} S_{i,j}(T)\, \phi_{i,j}(\nu) \right) \tag{2}$$

Where P is the system pressure, X is the specie mole fraction, $S(T)$is the absorption linestrength and ϕ is the lineshape broadening function. The last two parameters, $S(T)$ and ϕ, are discussed in the following sections and are key to the absorption feature and contain much of the thermodnamic information of the gas. The absorption coefficient simplified for a single specie:

$$\alpha(\nu) = P \cdot S_i(T) \cdot \phi_i(\nu) \tag{3}$$

1.2 Linestrength, S(T)

The linestrength of a ro-vibrational transition occurs at one specific frequency. The magnitude of this linestrength gives an indication of how strong a certain molecule's absorption will be when its dipole moment energy is activated by a photon of the same energy, hλ. Linestrength data are readily accessible thanks in a large part to experimental efforts to map these transtions at a reference condition (normally room temperature). One particularly popular archive of such data is the HITRAN molecular database [2]. HITRAN has an extensive log of many atmospheric and combustion species taken from collective experimental data as well as some extrapolated calulated values to fill certain gaps that are, as of yet, unattained by experimental methods. Figure 4 represents reference linestrength data for some common atmospheric and combustion species.

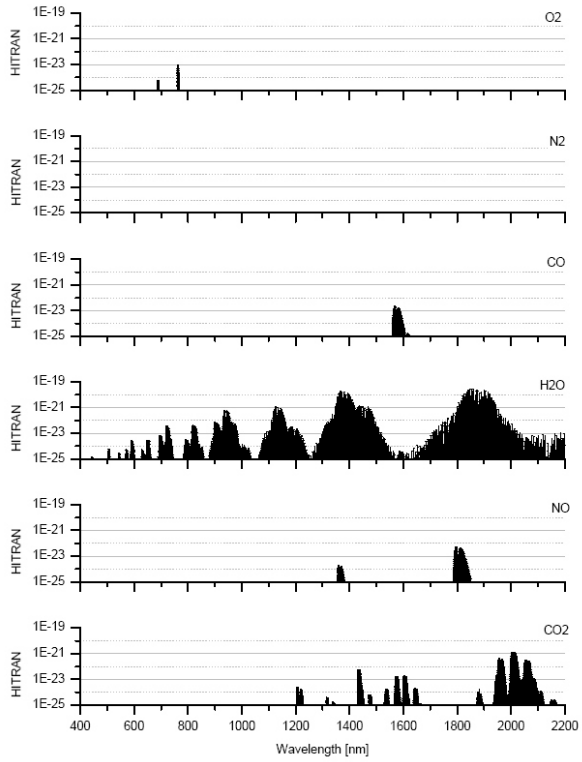

Figure 4: NIR linestrength spectra from HITRAN for some important atmosheric and combustion sepcies at 296K reference value

HITRAN linestrength units are given in $[cm^{-1}/molecule \cdot cm^{-2}]$ however a more convenient unit of $[cm^{-2}/atm]$ can be converted to via the relation in equation 4. Units throughout this report will have the potential to be in either of these units.

$$S\left[cm^{-2}/atm\right] = 7.34\,(10)^{21}\,\frac{1}{T}S^{*}\left[cm^{-1}/molecule\cdot cm^{-2}\right] \tag{4}$$

Scaling individual linestrengths can be done with equation 5. The key element in this relation in order to obtain accurate scaled values of $S(T)$ (aside from well measured reference values in HITRAN) is the partition function, $Q\,(T)$, which relates statistical and classical thermodynamic values. There exist accurate approximations for $Q\,(T)$, however, the accuracy of these models begin to wane for higher temperature cases [1, 2].

$$S_i\,(T) = S_i\,(T_0)\,\frac{Q\,(T_0)}{Q\,(T)}\left(\frac{T_0}{T}\right)\times\exp\left[-\frac{hcE_i''}{k}\left(\frac{1}{T}-\frac{1}{T_0}\right)\right]\times\frac{C\,(T)}{C\,(T_0)} \tag{5}$$

$$C\,(T) = 1-\exp\left(\frac{-hc\nu_{0,i}}{kT}\right) \tag{6}$$

An example of scaled linestrength values is illustrated in figure 5 which represents CO_2 scaled to 100K in the visible and near-IR spectrum. The inset plot illustrates a band near the $3\nu_1+\nu_3$ vibrational band centered at around 1605.68nm with individual rotational transitions. The rotational P-branch runs upward in wavelength from the band center of while the rotational R-branch runs downward in wavelength from the band center.

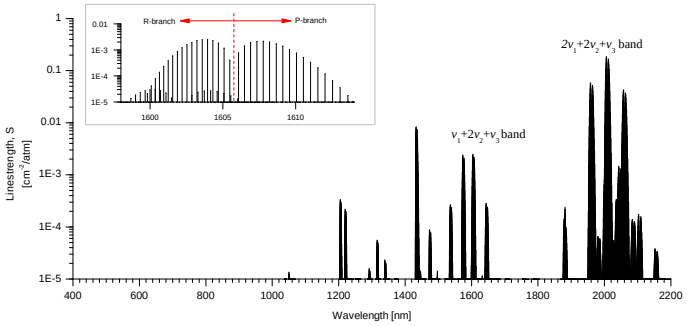

Figure 5: Linestrengths for CO_2 in the visible and near-infrared scaled to 100K via equation 5. The inset plot details a particular vibrational band with multiple R-branch (running left) and P-branch (running right) rotational transitions

1.3 Lineshape Broadening, ϕ

The linestrength of an single rotational absorption feature happens at one specific frequency but the absorption itself does not. This is owing to the fact that the absorption is statistically broadened over the line strength value via various broadening mechanisms. A couple of the most dominating broadening effects will be addressed here. Spectral lineshape broadening is denoted by, ϕ, and is defined with an total integral value of unity:

$$\int_{-\infty}^{\infty} \phi(\nu)\, d\nu = 1 \tag{7}$$

A more detailed analysis of many broadening effects can be found in reference [4].

1.3.1 Doppler Broadening, ϕ_D

The Doppler broadening, arising from the thermal velocity distribution of the probed gas, assumes the following Gausian model:

$$\phi_D(\nu) = \frac{2}{\Delta\nu_D}\left(\frac{\ln 2}{\pi}\right)\exp\left(-4\ln 2\left(\frac{\nu-\nu_0}{\Delta\nu_D}\right)^2\right) \tag{8}$$

where ν is frequency and ν_0 is the line center frequency of the absorption feature. The Doppler full-width half-maximum (FWHM) value, $\Delta\nu_D$, is found from:

$$\Delta\nu_D = \nu_0\left(\frac{8kT\ln 2}{mc^2}\right)^{\frac{1}{2}} \tag{9}$$

where m is the mass of the molecule, k is the Boltzmann coefficient, T is the temperature and c is the speed of light. Note that Doppler broadening is a function of temperature alone and no other thermodynamic parameter. This relation, simplified to work in frequency units of cm^{-1}, temperature units of K, and molecular mass of g/mole, is:

$$\Delta\nu_D = 7.162\times 10^{-7}\left[\nu_0\left(\frac{T}{M}\right)^{\frac{1}{2}}\right] \tag{10}$$

where M is the molecular mass of the molecule.

1.3.2 Collisional Broadening, ϕ_C

The model used for collisional broadening, due mainly to collisional interactions with other molecules, is the following Lorentzian-type distribution equation:

$$\phi_C(\nu) = \frac{1}{2\pi}\frac{\Delta\nu_C}{(\nu-\nu_0)^2 + \left(\frac{\Delta\nu_C}{2}\right)^2} \tag{11}$$

The self-broadened collisional FWHM, $\Delta\nu_C$, was determined from:

$$\Delta\nu_C = 2P\gamma_{self} \tag{12}$$

Values for the broadening coefficient γ were acquired from scaled values of data from the 2004 HITRAN database.

1.3.3 Voigt Broadening

Normally a broadened profile will not be purely Doppler or collisional in nature. A comparison of a Gaussian and Lorentzian distribution with equal full-width half-maximum (FWHM) values is illustrated in figure 6. This clearly shows the possible variety of broadening between a purely Doppler and a purely collisional profile. When this is the case one must consider a convolution of the two in the form of the Voigt function. The Voigt profile in equation 13 is considered for conditions where both collisional and thermal broadening effects are important.

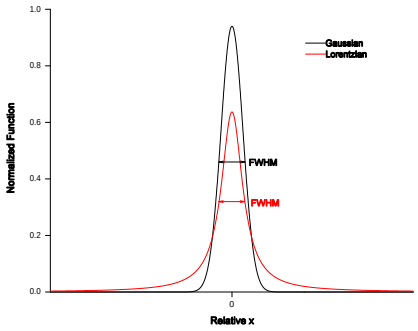

Figure 6: NIR linestrength spectra from HITRAN for some important atmosheric and combustion sepcies at 296K reference value

$$\phi_V(\nu) = \phi_D(\nu_0)\, V(X, Y) \tag{13}$$

where $V(X, Y)$ is the Voigt function with:

$$X = \frac{2\sqrt{\ln 2}\,(\nu - \nu_0)}{\Delta\nu_D} \tag{14}$$

$$Y = \frac{\sqrt{\ln 2}\Delta\nu_C}{\Delta\nu_D} \tag{15}$$

and Doppler broadened lineshape at linecenter, ν_0:

$$\phi_D(\nu_0) = \frac{2}{\Delta\nu_D}\left(\frac{\ln 2}{\pi}\right)^{\frac{1}{2}} \tag{16}$$

The Voigt function was acquired using the following analytical approximation [3]:

$$V(X, Y) = \sum_{i=1}^{4} \frac{C_i\,(Y - A_i) + D_i\,(X - B_i)}{(Y - A_i)^2 + (X - B_i)^2} \tag{17}$$

The constants A_i, B_i, C_i and D_i are given in table 1.

Table 1: Voigt model coefficients

	A	B	C	D
1	-1,2150	1,2359	-0,3085	0,0210
2	-1,3509	0,3786	0,5906	-1,1858
3	-1,2150	-1,2359	-0,3085	-0,0210
4	-1,3509	-0,3786	0,5906	1,1858

1.3.4 Determining appropriate broadening mechanism

Choosing an approriate broadening model to fit data is paramount to accurate measurements. Which criteria should one use when selecting a fitting model? The best means to tackle this problem is to fit various models and choose the one which generates the lowest residual values. Of course, there exist cases where values of $\Delta\nu_D$ is far larger than $\Delta\nu_C$ as in high temperature combustion and plasma applications. But more often than not, Voigt profiles are the preferred fit.

2 Tunable Diode Laser Absorption Spectroscopy

A simple TDLAS experiment is illustrated in figure 7.

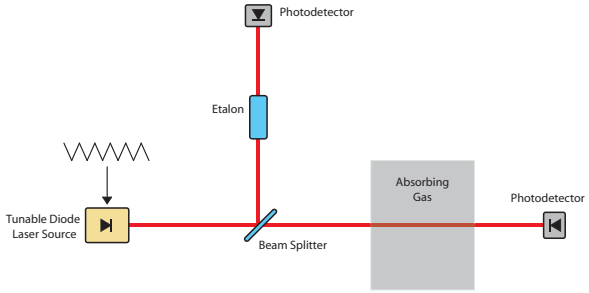

Figure 7: Simple TDLAS set-up incorporating an etalon as an interferometer for frequency tracking. The saw-tooth sketch represents a voltage or current signal used to drive the tuning mechanism of the laser.

The varying frequency output of a tunable diode laser is directed through an absorbing medium with the transmission signal, I, being recorded by a photodetector. An etalon signal taken before the absorbing gases for frequency tracking is also acquired. The etalon is used as a frequency marker in time in order to transfer absorption data from the time domain to frequency. When light is tuned through an etalon, which is basically two parallel flat plates, an interference pattern, like in the left-hand plot of figure 8, will occur. The spacing between two adjacent peaks, highlighted by the circles, is known to indicated the constant free spectral range (FSR) of the etalon. When plotting the peak occurances with time one can arrive at the transfer function plot on the right-hand side of figure 8. This data along with the knowledge of the FSR value of the etalon (1.54GHz for the case in figure 8) gives the important means to

acquire scans in frequency space.

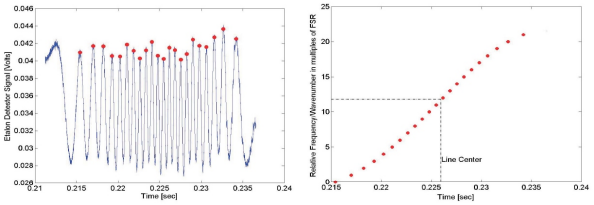

Figure 8: Using single scan etalon data to create transfer function data in FSR increments as a function of time.

In order to calculate the absorption for this experimental configuration, $-ln(I/I_O)$, a reference intensity must be acquired. One common technique involves the fitting of a baseline refernce to the transmitted intensity with the absorptionsignals cut out. Figure 9 illustrates this concept. A transmitted signal with two absorption features is recorded. The several present absorption features are identified with trimming indicies marked to exclude the absorption feature and wing data that could contaminate an ideal baseline fit (plot A). Those data points with the influence of absorption are removed (plot B) and fitted with an appropriate model (plot C). This fit represents the reference intensity, I_0, and now the absorption can be calcualted via $-ln\left(\frac{I}{I_0}\right)$ (plot D).

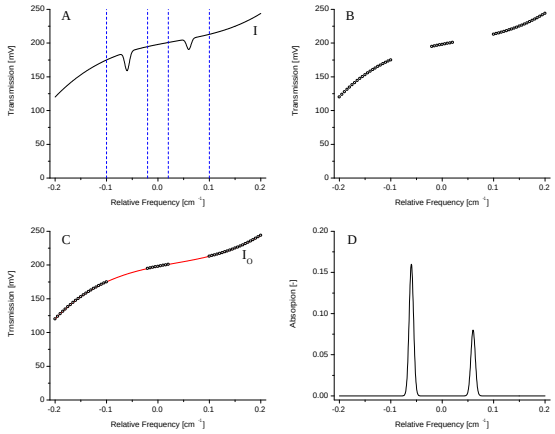

Figure 9: Baseline fitting data reduction technique A: Trimming locations in transmission signal, I B: data points used for baseline fit C: Baseline fit I_0 D:Absorption calculated from the relation $-ln\left(\frac{I}{I_0}\right)$

This technique of baseline fitting simplifies the experimental process by freeing up one channel of data acquistion as well as reducing the amount of optics and detectors required for the experiment.

2.1 Retrieving Thermodynamic Data

The key initial step in measuring the thermodynamic information is to acquire the temperature of the probed species. Bear in mind that this technique is an integrated line of sight measurement yielding a spatially averaged temperature. Thus, a constant temperature over the abosbing pathlength is desired, however, Abel inversion and other techniques have been used to measure non-uniform temperature distributions [20, 14]. The gas temperature can be determined in two fashions. If the temperature is high enough to assume a purely Doppler broadened profile, the the FWHM value can be used to directly extract the temperature from equation 9. If the profile is not purely Doppler then one can take advantage of the ratio of peaks between two profiles (figure 10) via the relation in equation 18 where the subscripts i and j represent the two transitions. The value of $area_i$ and $area_j$ simply represents the integrated absorbance of the indivdual features and S_0 represents the peak value of the feature. It is also important to note that the lower energy states must not be the same ($E_i'' \neq E_j''$).

$$T_{ij} = \left[\frac{1}{T_0} - \frac{1}{1.44\left(E_i'' - E_j''\right)} ln\left(\frac{area_i}{area_j} \frac{S_{0j}}{S_{0i}} \right) \right]^{-1} \tag{18}$$

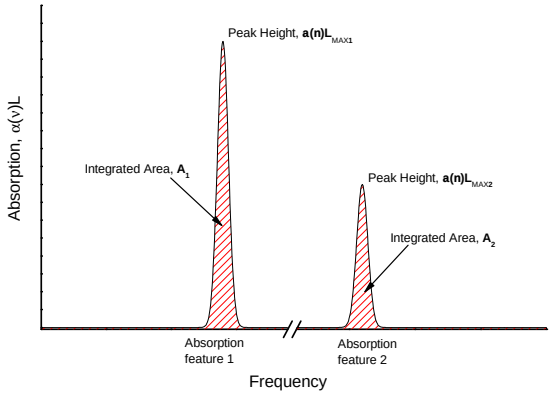

Figure 10: Illustration of two aborption peaks used for peak-ratio thermography

Even with the path integrated value of temperature being measured, this technique is significantly more meaningful in the monitoring of combustion health than combustor wall temperature monitoring with a thermocoupled imbedded in the wall even when the temperature is slightly non-uniform [12]. Choosing appropriate transitions for said temperature measurements will also need significant analysis to ensure adequate sensitivity for accurate measurements over the expected temperature ranges.

The species concentrations and gas pressure can be acquired once the temperature has been determined. The most simple method is by using the relation of the feature's integrated area of absorbance. Equation 19 shows this relation

as a function of pressure, P, species mole fraction, X, linestrength of transition i, $S_i(T)$, and absorption pathlength, L. The linestrength value can be acquired from equation 4 from the temperature.

$$area = P \cdot X \cdot S_i(T) \cdot L \tag{19}$$

2.2 Measuring Velocity

Measuring velocity can be done by taking advantage of the Doppler effect that occurs on the gas in motion with respect to the laser frequency. If the light source is at an angle to the flow, the absorption feature will be shifted by an amount $d\nu$ as shown in equation 20 where ν_0 is the feature line center, u_{gas} is the gas velocity, θ is the angle between the flow and the light source and c is the speed of light.

$$d\nu = \nu_0 \frac{u_{gas}}{c} cos\theta \tag{20}$$

One of the more accurate methods of acquiring velocity with TDLAS can be done with either the direct absorption signal or the harmonic signal using a 2-beam approach angled to the flow leading to double the Doppler shift in frequency space of the signal. Figure 11 illustrates this concept and is well documented to having low uncertainties even in subsonic flow [5].

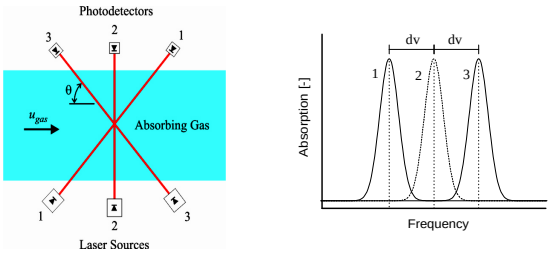

Figure 11: Simple velocity measurement experiment showing "rested" beam path (beam 2) perpindicular to flow direction for no Doppler shift, forward beampath (beam 1) for forward Doppler shift, and backward beam path (beam 3) for rearward Doppler shift

2.3 Modulation Spectroscopy

Modulation spectroscopy falls into two groups known as wavelength modulation spectroscopy (WMS) and frequency modulation spectroscopy (FMS). The main difference is the ampitude and frequency of the modulation to the laser voltage or current. In WMS, the amplitude of the dither is around the size of the FWHM value with a frequency on the order of 10kHz whereas in FMS, the amplitude is much smaller with frequencies on the order of 100MHz. This report will focus only on the more practical WMS approach. So what is meant by the dither of the voltage or current signal? Figure 12 illustrates this point

with a simple tuning voltage in the form of a linear low frequency ramp. The dither signal would be a higher frequency signal and some amplitude, a. Summing these signals together yields the dithered tuning signal driving the laser for WMS techniques.

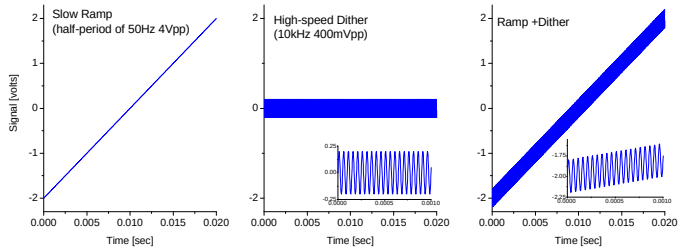

Figure 12: Ramp signal with added high-frequency dither

Modulation spectroscopy treats the absorption feature as a Taylor sum of the derivatives of the signal. This is why the technique is sometimes reffered to as derivative spectroscopy. The most common signal to analyze is the 2nd harmonic or $2f$ signal (figure 13). Though, experimentally the "mexican hat" $2f$ signal will be contaminated by the $1f$ and $3f$ signal, the peak of the $2f$ signal will always remain at the line center of the direct absorption feature. This is owing to the fact that the $1f$ and $3f$ signals are zero at the line center. It is this characteristic of the $2f$ signal that makes it the optimum choice for harmonic detection s opposed to the $1f$ or $3f$ signals whose line center values are much more difficult to identify. Acquiring the harmonic signals is done with lock-in amplification. The modulated transmitted signal from a photodetector is sent to a lock-in amplifier with the dither frequency as a reference input. This lock-in amplifier then is able to filter and extract the $2f$ signal.

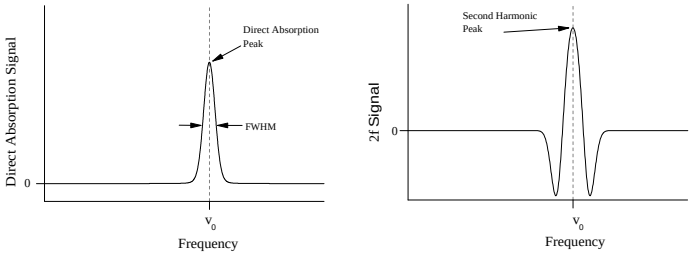

Figure 13: Direct absorption signal conversion to a typical "Mexican Hat" shaped second harmonic (2f) signal. Both tuning frequency scales are identical

The key to acquiring an adequate $2f$ signal lies in the proper choosing of the modualtion depth, a. The modulation depth can be related to the modulation index, m, by the relation in equation 21. An optimal value of a for where the peak of the $2f$ signal is at a maximum occurs when $m \sim$2.2 as illustrated in

figure 14. This yields a relation of an optimal a as a function of the FWHM value of the direct absorption feature (equation 22) which is a key result for WMS techniques. However, one must have a estimate of the direct absorption FWHM value a priori.

$$m = \frac{a}{\frac{1}{2}\Delta\nu_{FWHM}} \tag{21}$$

$$a_{optimal} = 4.4 \cdot \Delta\nu_{FWHM} \tag{22}$$

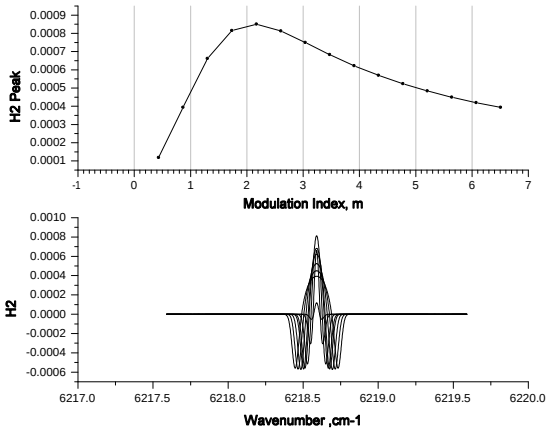

Figure 14: 2f signals for various values of modulation index, m

The experimental set-up in figure 15 was used to illustrated the experimental benifits of using harmonic detection by attempting to detect the levels of CO_2 in ambient air. Figure 16 is a simulation of CO_2 in ambient air at 300ppm mole fraction with a pathlength, L, of 150cm to estimate a value for a. The linestrength values and Voigt broadened profile were done at room temperature. The level of absorption is clearly seen to be quite small, at 0.005% absorption. This implies only a 0.005% change in transmitted intensity signal. For the purpose of illustration, assume this direct absorption signal had an original baseline level, I_0, of 1V and a noise band of 1mV. This would yield a 0.1% noise band resulting in a S/N ratio 0.05 making it completely impossible to measure using the previously discussed direct absorption technique. However, this very small concentration of CO_2 was easily detected in both illustrated scans with the WMS technique.

There are drawbacks to WMS owing to the fact that the original signal with the most important thermodynic information is more or less destroyed. Directly utilizing the FWHM values and integrated areas to measure temperature, pressure, and species concentration is not possible. However, peak ratio thermography as well as analyzing the Doppler shifting of peaks to measure velocity is still possible and in many cases more accurate than the direct absorption approach [16].

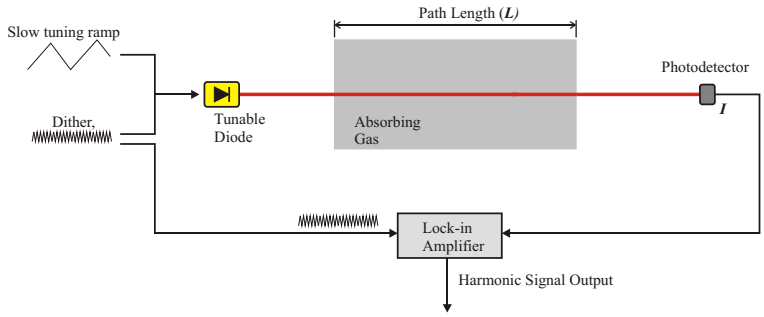

Figure 15: Experimental setup for WMS

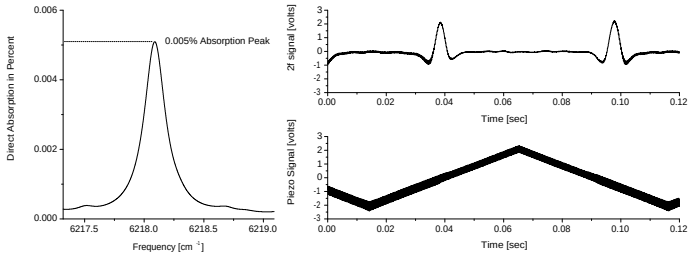

Figure 16: Left plot: Direct absorption simulation of 300ppm CO_2 mole fraction in ambient air for a 150cm pathlength. Right plot: second harmonic WMS detection in ambient air over a 150cm pathlength. Slow ramp frequency was set to 10Hz while the dither amplitude frequency at 3.5kHz and a modulation index of about 2.2

3 Application Example: VKI Longshot Facility Measurements of CO_2

3.1 Longshot Facility

In 1967, the von Karman Institute brought the Longshot piston driven impulse hypervelocity facility into operation (figure 17). A driver section is filled to high pressure and is separated from the driven section via an aluminum rupture diaphragm, which supports the piston. The driven section is kept at an intermediate pressure between the driver section and evacuated nozzle and test section pressures. A second diaphragm is used to separate the driven tube from the evacuated nozzle/test section. The piston is released when excess nitrogen is bled from the circumference of the primary diaphragm. A shock travels ahead the piston, which is traveling around 600m/s. When this preceding shock reflects off of the end of the barrel, it will reflect off of the piston subsequently slowing it down. This process of reflection repeats back and forth until the piston stops and then begins to travel back towards the driver tube. This would create a back flow if it were not for a series of check valves before the reservoir only allowing flow in the direction towards the plenum. The

gas that is forced into the plenum, which can reach pressures as high as 4000 bar, is then fed through a convergent divergent nozzle accelerating the gas to high velocities. This nozzle was a simple axisymmetric conical nozzle until it was replaced in 1990 by an axisymmetric contoured nozzle. At the end of the tunnel is a 3m diameter test section with a 5 axes positioning mechanism for model orientation and support. Detailed analysis of the facility can be found in [17, 18].

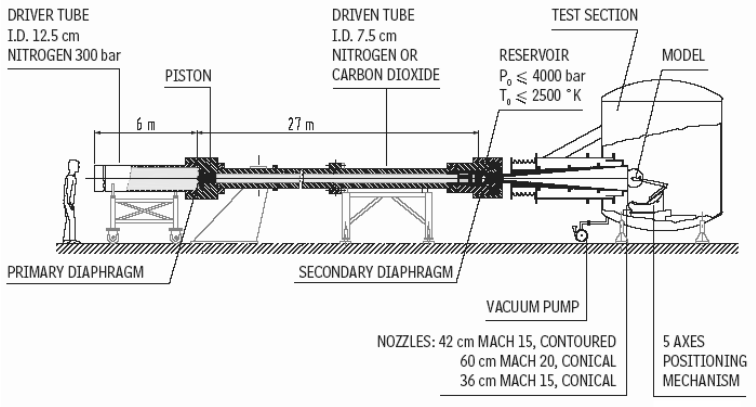

Figure 17: Longshot piston driven impulse hypervelocity facility

3.2 Objective

The objective of applying TDLAS to the Longshot facility is to characterize the free-stream properties of the facility while running CO_2. This work will greatly aid in the study of real gas effects on the CO_2 flow in the Longshot facility. Owing to the high pressure conditions in the plenum, the ideal gas equation of state:

$$PV = nRT \tag{23}$$

can no longer be assumed for simple thermodynamic calulations. Even with the more accurate Van der Waals equation, current Longshot data reduction techniques by using Fay-Riddel theory still lead to 30 to 40% uncertainty in free stream static pressure and temperature measurements [19, 18]. It is desired to use the TDLAS technique to more accurately characterize the flow conditions and compare to traditional data reduction techniques. These results will also help to improve upon CFD simulations where the same problems and errors arise.

There is also an issue with the TDLAS technique being an integrated line of site measurement. Figure 18 illustrates the regions where non-uniform density occurs. The region labelled δ arises from the build up of the boundary layer inside the nozzle and the shear layer characteristic of the flow. Another region of concern is the region out of the flow from the nozzle. In the regions just after the laser output up until the edge of the flow and just after the flow up until

the photodetector there can be additional absorption owing the accumulation of the test gas in the test cabin of the facility. Section 3.5 addresses this issue and illustrates a concept to ensure the aborption only occurs in the constant core flow.

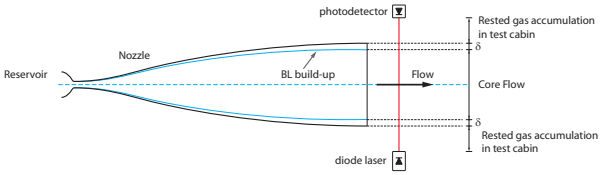

Figure 18: Illustration of non-uniform density regions typical in impulse hypervelocity facilities.

3.3 Sensor Design

In order to aquire an accurate absorption measurement, preliminary investigation into available laser systems coupled with a simulated analysis of the absorption process in the Longshot facility must be addressed. Figure 19 represents the now familiar CO_2 ro-vibrational spectra at 100K. Superimposed are laser tuning ranges for specific external cavity diode laser (ECDL) models from the New Focus laser company.

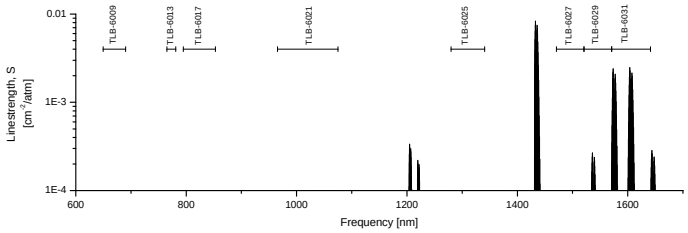

Figure 19: Simulated CO_2 spectra of the 4th overtone ro-vibrational band for approximate Longshot free-stream conditions

The selected laser was the one with the most potential, TLB-6031 laser sytem (table 2 for general details), with peak linestrengths, S, near 1600nm at around 2E-3[cm^{-2}/atm] at 100K. However, 100K is a measured Longshot condition with nearly 40% uncertainty. Figure 20 illustrates the P10, P12 and P14 ro-vibrational transition linestrengths for 60K up to room temperature. Clearly, the three transitions remain relatively strong even in the uncertainty range for Longshot free-stream temperature measurements. The fact that it was desired also to have a potential CO transition in the tuning range for future plasma tests led to choosing a tuning range to incorporate the P12 transition. Though ECDLs offer a large tuning range, the New Focus Vortex series laser must be set

to a much smaller tuning range in order to incorporate the high-speed tuning which is a drawback for high speed tuning ECDLs. Data for the TLB-6031 laser with the appropriately set tuning range to incoporate the P12 transition can be found in table 3.

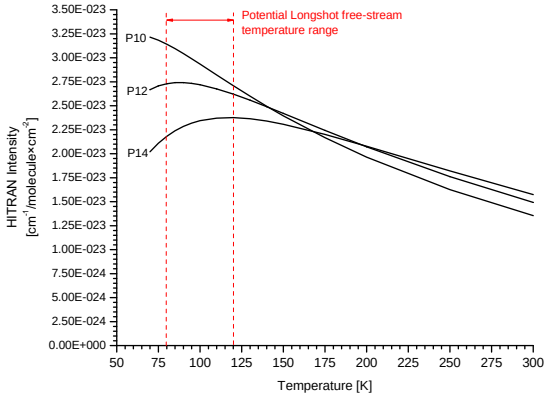

Figure 20: Linestrengths for laser tuning range consideration

Figure 27 represents the simulated spectra of the 4th overtone ro-vibrational band of CO_2 at approximate Longshot freestream conditions. The location and width of the laser tuning range is illustrated as well and is shown to include the P12 transition. The inset graph shows the characteristic temperature and pressure broadened feature which contains relavant thermodynamic information. The free-stream temperature and pressure can be measured with typical transducers as stated before but a large uncertainty risk of nearly 40%. In figure 22 one can easily see the potential range of absorption features assuming a Voigt profile.

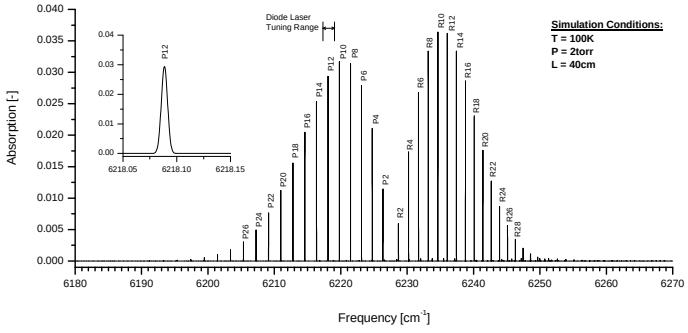

Figure 21: Simulated CO_2 spectra of the 4th overtone ro-vibrational band for approximate Longshot free-stream conditions. Inset plot represents probed P12 transition

Table 2: New Focus Vortex 6031 tunable diode laser capabilities

Available Wavelengths	1.570um to 1608.41um (6369 to 6098cm^{-1})
Tuning Range	30GHz (just over 1cm^{-1})
Modulation Band Width	3.5kHz
Linewidth	less than 300kHz
Typical Power Range	5 to 15mW
Current Modulation Frequency	50kHz - 100MHz
Frequency Modulation	
Max. Voltage	$\pm$4.5V
Input Frequency Range	DC-3.5kHz
Impedance	5kΩ
Current Modulation	
BNC Input	
Max. Voltage	$\pm$10V
Input Frequency Range	DC-1MHz
Impedance	5kΩ
Moduation	0.2mA/V
SMA input (high-speed)	
Max. Voltage	1V$_{p-p}$
Input Frequency Range	50kHz-100MHz
Impedance	50Ω
Moduation	20mA/V

Table 3: Set laser tuning range

	λ[nm]	$\bar{\nu}$ [cm^{-1}]	ν [GHz]
	1607.96	6219.09	1.86443×10^5
	1608.41	6217.32	1.863906×10^5
Range $\Rightarrow$	0.45	1.77	52.4

A portable bench containing all the optics necessary on the pitch side of the optical assembly on a small breadboard (30cm x 40cm) was created to facilitate the ease of porting the experiment from absorption cell to facility and vice versa. Figure 23 illustrates this set-up. In order to further increase the portability of the system, optical fibers were incorporated. The decision was to use single-mode fibers due to their low modal dispersion characteristics. However, this introduced the challenge of coupling a 2mm diameter free-space beam into a 9μm fiber core. A Newport model F-91-C1 single mode fiber aligner with an Optics for Research (OFR) model LLO-4-7-IR coupling objective (NA=0.30) was used to focus the light into the 5m steel re-enforced jacketed single mode fiber (NA=0.15) with an angled physical contact (APC) end to prevent backreflections into the laser cavity. This numerical aperture "mismatch" was chosen on purpose to create a steeper half cone angle of light approaching the optical fiber to reduce beam waist diameter, and this led to a higher coupling efficiency than trying to match NA values directly. A small portion of the light (about 8%) was picked via a pellicle off beam-splitter before heading to the fiber aligner and guided through an etalon to acquire a frequency marker. Nearly 65% of

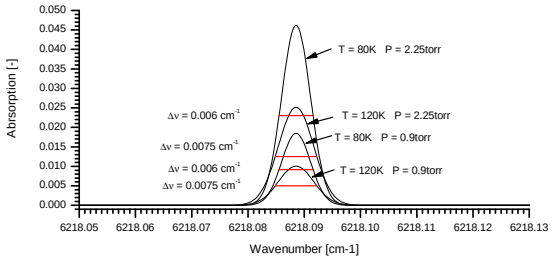

Figure 22: Longshot freestream absorption calculations with 40% temperature and pressure uncertainty from traditional experimental measurement techniques

the laser power is coupled into the fiber with this configuration. The etalon has a free-spectral range (FSR) of 1.59GHz near 1600nm and was sufficient in the full laser tuning range to acquire around 25 peaks for transfer function data. The light passed through the etalon was detected via a Thorlabs DET410 high-speed photodetector with a spectral response of 700-1800nm, an active area of ϕ1mm and a rise/fall time of 5ns.

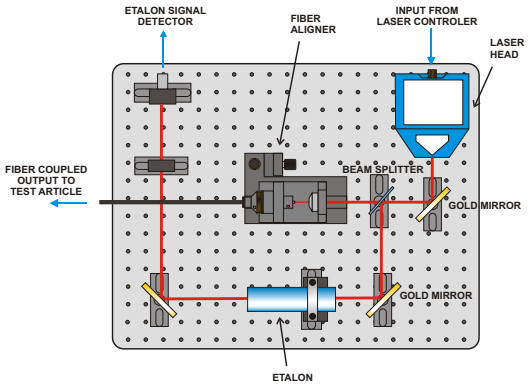

Figure 23: Portable breadboard for simple pitch portability

3.4 Preliminary Results

Preliminary results demonstrate that direct absorption techniques are capable of detecting free-stream CO_2 in the Longshot facility without the need to resort to $2f$ harmonic detection. These results, however, were done at a sampling resolution of only 62.5kS/sec per channel albeit at 16-bit resolution. Even zooming in as far as possible and only tuning the laser at 150Hz (300 laser scans per second) it is not possible to resolve the absorption feature well enough to accurately fit the feature to a Voigt profile for data reduction purposes. The experimental set-up utilized the portable optical bench with single mode fiber

output from a fiber with a steel jacket re-enforcement (section 3.3). This was then attatched to a colimator with gimble mount for beam steering that was magnetically 'fixed' to a heavy Schlieren mirror base. On the other side of the cabin a gold mirror was mounted to reflect back the light through the cabin for a double pass measurement. This in theory decreases the S/N ratio since with each pass of the windows there is a loss of power owing to reflections but it was assumed that the advantage of doubling the absorption outweighed this drawback. The light was then collected right next to the pitching colimator with a simple lens-detector configuration, both of which were mounted with magnetic bases. The beam divergence was minimal with this collimator at about 0.05deg. Figure 24 illustrates this set-up.

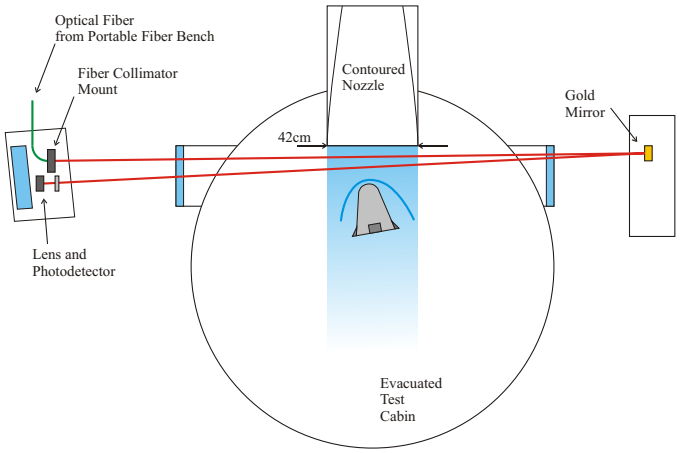

Figure 24: Longshot experimental set-up for initial direct absorption tests with double-pass conifguration. All optics are installed outside of the test cabin.

Two tests were made with the optics outside of the test cabin. The first test was a single-pass test with the laser tuning range at the maximum to more porperly identify the abosrption features. In this configuration a weak CO_2 signal was acquired with very low sampling resolution. The next test was done with a double pass configuration with the laser tuning range set to the center of the absortion feature while narrowing the tuning range around the absorption to acquire more data points over the feature. The limit of zooming is based not only on the width of the absorption feature but as well as the FSR of the etalon. Too few peaks would make it difficult/impossible to retieve an accurate representation of the feature in frequency space. Five etalon peaks per scan are the lower limit desired. Figure 25 represents the full unreduced data set from the double pass test. The uppermost plot represents the transmission signal acquired from the photodetector mounted on the Schlieren mirror base. The second sinusoidal trace is that of the voltage controlling the piezo which is the tuning mechanism for the laser. One forward laser scan is from a peak to a neighboring trough in the signal. A subsequent reverse scan is from a trough to a peak and so on. Thus, there are 2 scans (one forward and one reverse) to each period of the tuning sine waveform implying 300 scans per second for a 150Hz tuning frequency. A sinewaveform was used rather than a saw-tooth waveform in order to reduce the stress on the piezo at the turning

point (peak and trough value). The third plot is a total pressure trigger (which was saturated but still served its purpose) from a total pressure probe, P_{t2}, inserted into the freestream. The test is considered to start at the sharp pressure rise from this signal. The last signal is that of the etalon interferometer for frequency tracking.

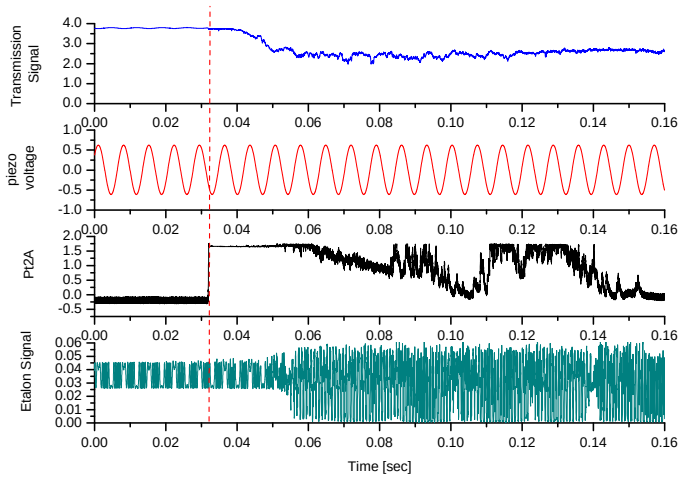

Figure 25: Longshot raw data from double pass test case

After the test begins (at 32ms), it is easy to see a drop in signal starting around 40ms. This initial drop is due to optical misalignment from the beam steering with the density gradient of the gas entering the test cabin. However, at this viewpoint it is impossible to indicate any abosorption features. Upon zooming into the first four scans (figure 26) one can more clearly see what is happening. In each scan, a significant dip in the location of where CO_2 should be is present after the test begins where there is none before the test. This is clearly owing to the CO_2 of the free-stream gas in the Longshot cabin. The data sampling continued for 160ms but vibrations completely ruined the signal after about 47 to 48ms.

The two test results (one single-pass and one double-pass) in an attempt to measure CO_2 free-stream properties are plotted in figure 27. The first test was a single pass attempt with the laser tuning range at the maximum to positively identify the absorption feature. As it can be seen, this features strength is quite small and the shape of the feature is not very well resolved. The tuning range of the laser was then windowed in closer to the absorption feature in the double-pass case yielding to the higher number of data points over the absorption feature. In this case, the peak was more well resolved leading to a greater than a doubled amplitude from the single-pass case.

However, the higher sampling rate is still not enough. The 10 or so data points constructing the meat of the absorption feature still lead to large fitting errors. Current data reduction yields about 140K and 1.9 torr if one were to assume a pure Doppler fit.

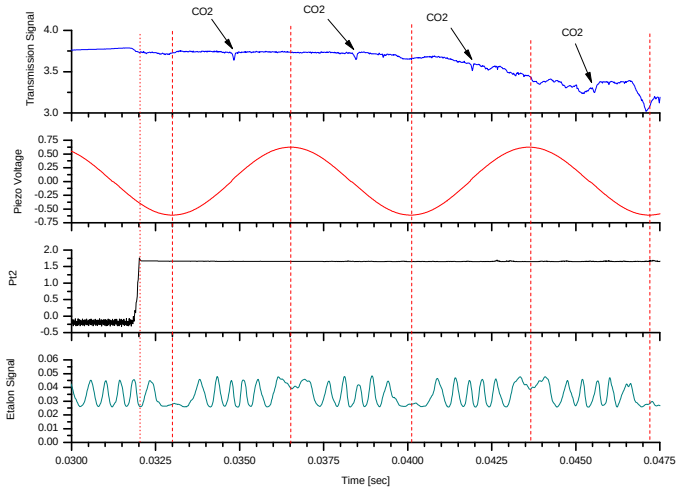

Figure 26: Longshot raw data from double pass test case zoomed to first four scans. The first vertical line represents the event triggering the data acquisition. The four subsequent vertical dashed lines are serparators between individual scans.

3.5 Near-future Work

A new data acquisition card (National Instruments NI-6120) with a sampling rate of 1MS/sec per channel at 16-bit resolution has been incorporated into the data acquisition system. Further results will be presented once the absorption feature has been well resolved with the new DAQ card and removed from any shear layer distortion via the shear layer shields. A preliminary concept of said shields can be seen in figure 28 for a two-beam approach. The concept is to insert a flat plate with a wedged front face with a NIR optically transparent material into the core flow to prevent the absorption feature from having any the influence from the nonuniform density regions. The developing boundary layer and resulting shock for hypersonic flow will be quite small as the boundary layer thickness scales with $M_\infty^2/\sqrt{Re_x}$. This concept will be incorporated into the newly installed optical support frame (figure 29) which is intended to support all pitching optics catching optics. The portable optics bench will be set outside of the test cabin with light delivered from a fiber optic fed to the pitching optics on the support frame. Figure 30 illustrates the predicted absorption feature shift with respect to the "rested" feature for various angles with respect the the core flow direction. Velocity measurements ar expected to have a $\pm$25m/s error even with a modest angle of $\pm$20deg.

4 Concluding Remarks

The TDLAS technique described in this work provides a foundation for the development of measurements systems for many flow applications [16, 15, 9, 14].

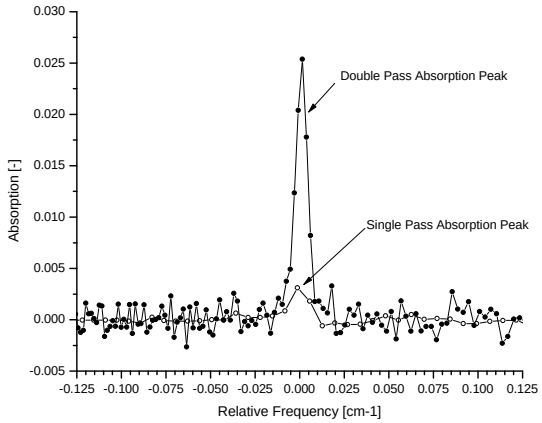

Figure 27: Comparison of two free-stream CO_2 absorption profiles in the Longshot facility at 62.5kS/sec sampling rate.

TDLAS has proven to be a rugged laboratory tool as well as a strong remote sensing contender to traditional intrusive probing techniques in hostile enironments. The field is a rapidly growing field one and with the emergence of quantum cascade lasers (QCL) more an more stronger fundamental bands are becoming available deeper into the IR and beyond the telecommunications corridor [20, 21] opening up many more sensing possibilities. The ability of these techniques are opening up to a wide variety of applications ensuring a steady growth of the field well beyond the capabilities illustrated here.

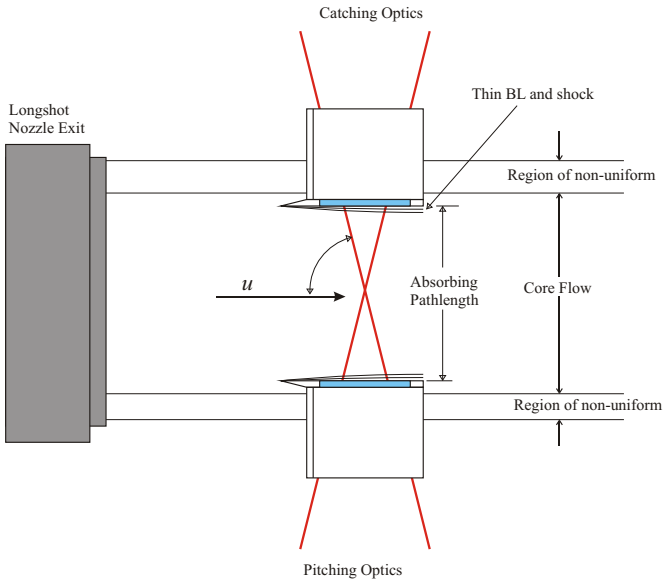

Figure 28: Two-beam Doppler shift comparison for various angels for Longshot free-stream conditions

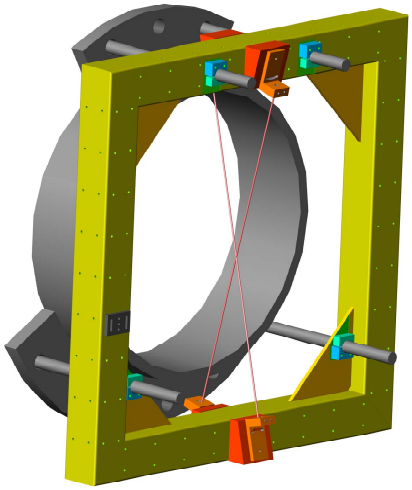

Figure 29: Recently installed Longshot optical support framewith two angled beam approach

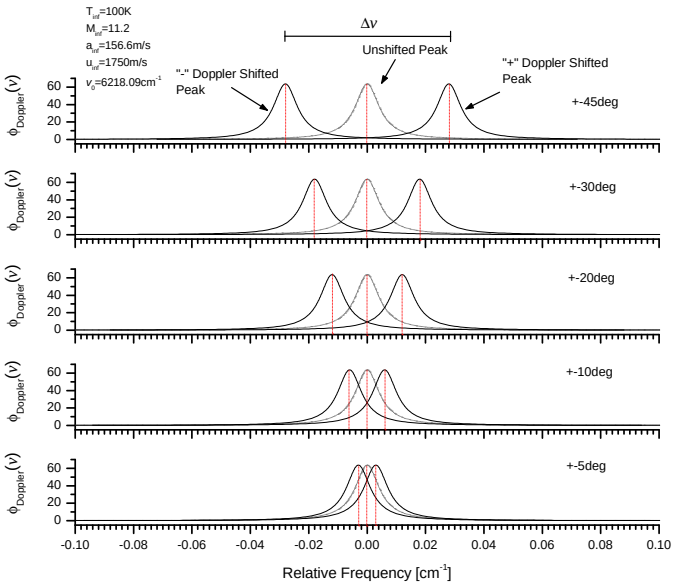

Figure 30: Two-beam Doppler shift comparison for various angels for Longshot free-stream conditions

References

[1] L. S. Rothman et. al, "The HITRAN molecular spectroscopic database: edition of 2000 including updates through 2001", Journal of Quantitative Spectroscopy and Radiative Transfer, (2003) 85:5-44

[2] L. S. Rothman et. al, "The HITRAN 2004 molecular spectroscopic database", Journal of Quantitative Spectroscopy and Radiative Transfer, 96 (2005) 139-204

[3] A. B. McLean, C.E.J.Mitchell and D.M.Swanston, Implementation of an efficient analytical approximation to the Voigt function for photoemission lineshape analysis, Ultramicroscopy, (2002).

[4] W. Demtroeder, "Laser Spectroscopy"

[5] K. Lyle, "Development of a Real-time Diodelaser Mass Flux Sensor for Simultaneous MEasurement of Density and Velocity of Oxgygen", Report No. TSD-163, High Temperature Gasdynamics Laboratory, Thermoscience Division, Department of Mechanical Engineering, Stanford University, 2005

[6] Newfocus, "FM Spectroscopy with Tunable Diode Lasers", Application Note 7, New Focus Corporation, www.newfocus.com

[7] A. Y. Chang, E. C. Rea, Jr., and R. K. Hanson, "Temperature Measurements in Shock Tubes Using a Laser-Based Absorption Technique," Applied Optics, Vol. 26, 885-891 (1987)

[8] A. -K. Mohamed, D. Henry, J. -P. Falni, P. Sagnier, J. Soutad, W. H. Beck, J. Martinez Schramm, "Infrared Diode Laser Absorption Spectroscopy Measurements in the S4MA, F4 and HEG Hypersonic Flows," International Symposium on Atmospheric Reentry Vehicles and Systems, 16-18 March 1999, Arcachon, France

[9] A. -K. Mohamed, D. Henry, D. Bize, W. H. Beck, "Infrared Diode Laser Absorption Measurements in the HEG Free Stream Flow," paper no. AIAA-98-2870, 20th AIAA Advanced Measurement and Ground Testing Technology Conference, Albuquerque, NM, USA, 1998

[10] R. M. Mihalcea, D. S. Baer, and R. K. Hanson, "Advanced Diode Laser Absorption Sensor for In-situ Combustion Measurements of CO2, H2O, and Gas Temperature," paper no. AIAA 98-0237, 36th Aerospace Sciences Meeting and Exhibit, Reno, NV, USA, 1998

[11] S. Boege and T. Rossman, "Tunable Filter Absorption Spectroscopy for High Pressure Combustion Systems", paper no. AIAA 2007-465, 45th Aerospace Sciences Meeting and Exhibit, Reno, NV, 2007

[12] R. M. Mihalcea, D. S. Baer, and R. K. Hanson, "Diode Laser Sensor for Measurements of CO, CO2, and CH4 in Combustion Flows," Applied Optics, Vol. 36, No. 33, 8745-8752 (1997)

[13] R. M. Mihalcea, D. S. Baer, and R. K. Hanson, "Diode-laser Absorption Measurements of CO_2 near 2.0μm at Elevated Temperatures", Applied Optics, 37(36):8341-8347,1998

[14] T. I. Palaghita, "Combustor Exhaust Temperature Nonuniformity Sensing Using Diode Laser Absorption", PhD Dissertation, Daniel Guggenheim School of Aerospace Engineering, Georgia Institute of Technology, 2007

[15] R. K. Hanson and J. B. Jeffries, "Diode Laser Sensors for Ground Testing", paper no. AIAA 2006-3441, 25th AIAA Aerodynamic Measurement Technology and Ground Testing Conference 5-8 June 2006, San Francisco, California, USA

[16] J. Wang, "New Strategies of Diode Laser Absorption Sensors", Report No. TSD-141, High Temperature Gasdynamics Laboratory, Thermoscience Division, Department of Mechanical Engineering, Stanford University, 2001

[17] Simeonides, "The VKI Hypersonic Windtunnels and Associated Measurement Techniques", Technical Memorandum, The Von Karman Institute for Fluid Dynamics, 1990.

[18] J. -M. Charbonnier, S. Paris and W. Dieudonne, "Extension of the Operating Domain of the VKI-Longshot Tunnel to the Use of Testing Gases with Various γ Values," Technical Memorandum, von Karman Institute for Fluid Dynamics, Rhode-Saint-Genese, Belgium

[19] S. Laurent, "Numerical Simulation of Carbon Dioxide Flows in Hypersonic Wind Tunnel and in Atmosphere Reentry Conditions", Student Report, Von Karman Institute for Fluid Dynamics, 2004, Rhode Saint Genese, Belgium

[20] R. A. Parker, T. Wakeman, M. MacLean and M. Holden, "Measuring Nitric Oxide Freestream Concentration Using Quantum Cascade Lasers at CUBRC", paper no. AIAA 2006-926, 41st Aerospace Sciences Meeting and Exhibit, Reno, NV, 2006

[21] R. A. Parker, T. Wakeman, M. MacLean and M. Holden, "Measuring Nitric Oxide Freestream Velocity Using Quantum Cascade Lasers at CUBRC", paper no. AIAA 2007-1329, 45th Aerospace Sciences Meeting and Exhibit, Reno, NV, 2007